Geomechanics and Engineering, *Vol. 38, No. 4 (2024) 381-395*
https://doi.org/10.12989/gae.2024.38.4.381

Optimization of construction support scheme for foundation pits at zero distance to both sides of existing stations based on the pit corner effect

Tonghua Ling[1a], Xing Wu*[1], Fu Huang[1], Jian Xiao[1], Yiwei Sun[2] and Wei Feng[3]

[1]*Changsha University of Science & Technology, Changsha, China*
[2]*Shanghai Geoharbor Construction Group Co., Ltd., Shanghai, China*
[3]*China Construction Fifth Engineering Division Corp, Ltd, China*

(*Received July 6, 2023, Revised July 16, 2024, Accepted July 30, 2024*)

Abstract. With the wide application of urban subway tunnels, the foundation pits of new stations and existing subway tunnels are becoming increasingly close, and even zero-distance close-fitting construction has taken place. To optimize the construction support scheme, the existing tunnel's vertical displacement is theoretically analyzed using the two-stage analysis method to understand the action mechanism of the construction of zero-distance deep large foundation pits on both sides of the existing stations; a three-dimensional numerical calculation is also performed for further analysis. First, the additional stress field on the existing tunnel caused by the unloading of zero-distance foundation pits on both sides of the tunnel is derived based on the Mindlin stress solution of a semi-infinite elastic body under internal load. Then, considering the existing subway tunnel's joints, shear stiffness, and shear soil deformation effect, the tunnel is regarded as a Timoshenko beam placed on the Kerr foundation; a sixth-order differential control equation of the tunnel under the action of additional stress is subsequently established for solving the vertical displacement of the tunnel. These theoretical calculation results are then compared with the numerical simulation results and monitoring data. Finally, an optimized foundation pit support scheme is obtained considering the pit corner effect and external corner failure mode. The research shows a high consistency between the monitoring data,analytical and numerical solution, and the closer the tunnel is to the foundation pit, the more uplift deformation will occur. The internal corner of the foundation pit can restrain the deformation of the tunnel and the retaining structure, while the external corner can cause local stress concentration on the diaphragm wall. The proposed optimization scheme can effectively reduce construction costs while meeting the safety requirements of foundation pit support structures.

Keywords: deep and large foundation pit; external corner of foundation pit; Kerr foundation model; pit corner effect; support optimization; zero-distance construction

1. Introduction

Many deep and large foundation pit projects have emerged with the increasing construction of medium and high-rise buildings, underground pipe galleries, and subway stations. The frequency of foundation pit construction near existing tunnels is gradually increasing, and there are more and more close-range even zero-distance construction, presenting a challenge to traditional design and construction technology (Ding *et al*. 2018). The unloading of the foundation pit during excavation will inevitably cause disturbance to the surrounding soil, leading to uneven settlement or uplift deformation of the existing tunnel (Liang *et al*. 2017). When the deformation is too large, the surrounding wall can easily lose its support, causing instability and falling off, posing a great threat to the existing tunnel's safe operation. Meanwhile, if the support system is designed to be conservative, for example, increasing the thickness of the diaphragm wall and the number of internal supports. However, this design would significantly increase construction costs (Liu *et al*. 2021).

Currently, the main research methods used to overcome the deformation of existing tunnels caused by excavating foundation pits include on-site detection, numerical simulation, and theoretical calculation methods. The on-site detection method is one among the most commonly used by researchers (Liu *et al*. 2021, Cai *et al*. 2016, Liu *et al*. 2014). For example, Mei *et al*. (2021) analyzed the monitoring data of deep foundation pits of 15 metro stations in Shanghai, Ningbo, and Hangzhou and showed that the maximum lateral shift of the diaphragm wall was linearly related to the excavation depth of the foundation pit. Researchers analyzed the monitoring data of a soft soil deep foundation pit in Hangzhou, compared it with other similar foundation pits, and concluded that a ratio of foundation pit length to excavation depth within 3 could effectively restrict the deformation of the foundation pit (Ding *et al*. 2018, Yu *et al*. 2017). Although field observation and experimental research have been widely used, they are often limited by complex working procedures and high costs in engineering practice (Chen 2020).

Theoretical calculation method plays an important role in preliminary prediction because of its fast and simple steps (Zhang *et al*. 2020). Currently, the two-stage analysis method is the most commonly used theoretical calculation

*Corresponding author, Professor
E-mail: 21102020397@stu.csust.edu.cn
[a]Professor
E-mail: lingtonghua@163.com

ISSN: 2005-307X (Print), 2092-6219 (Online)

method. The equivalent stiffness coefficient of longitudinal bending is the key parameter for analyzing the longitudinal stress characteristics of existing tunnels using the two-stage analysis method. Li *et al*. (2021) proposed calculation models for the longitudinal bending stiffness of fillet rectangular Pipe-Jacking Tunnel (RPJT) based on the RPJT structural elements and further analyzed the influence of the number of longitudinal bolts and the thickness of the segment on the neutral axis position and the longitudinal equivalent stiffness. Based on the Mindlin stress solution, Wei *et al*. (2016) considered the influence of the foundation pit bottom and the retaining side wall and found that with a reduction in the distance between the pit and the existing tunnel, the shape of the additional stress curve changed from "straight" to "M", and the direction changed from vertical down to vertical up. Traditional models like the Euler-Bernoulli beam and Winkler foundation fail to account for the shear stiffness of existing tunnels and the shear interaction between soil and tunnels (Lohar *et al*. 2019, He *et al*. 2016, Limkatanyu *et al*. 2023). To enhance calculation accuracy, some researchers have adopted a two-parameter foundation model combined with a nonlinear volume model (Avcar *et al*. 2022; Bennedjadi *et al*. 2023, Zhang *et al*. 2023). Wang *et al*. (2022) utilized the Vlasov-Timoshenko beam foundation model to compute difference solutions under elastic boundary conditions by introducing translating and rotating constrained springs, considering soil spatial variability. However, the Vlasov foundation model, unlike the three-parameter foundation model, does not account for shear effects between soil masses (Huang *et al*. 2012). Zhang *et al*. (2019) then modeled the existing tunnel as a Timoshenko beam on a Kerr foundation to include the longitudinal shear stiffness, verifying their two-stage analysis method using centrifuge experiments and on-site data. They studied the effects of longitudinal shear stiffness, volume loss, and tunnel-soil relative stiffness coefficient on tunnel response. However, the mechanical behavior of foundation pit corners is rather complex, making it challenging to consider three-dimensional hardening in theoretical calculations (Szepeshazi *et al*. 2016). The pit corner effect, which causes minimal lateral or vertical displacement of the diaphragm wall near the foundation pit corner during excavation (Roboski 2004), can reduce construction costs by lowering support stiffness or reducing support components at the corner (Liu *et al*. 2021). Thus, understanding the pit corner effect's impact on foundation pit deformation is crucial for comprehensive risk assessment, design, and construction of deep and large foundation pits (Nam *et al*. 2022).

The pit corner effect is essentially an arching effect phenomenon caused by uneven deformation of soil around the pit in a three-dimensional state (Li *et al*. 2014). One of the main research methods to study this complex pit corner effect is the numerical analysis method. Based on an irregular foundation pit project in Xiamen, researchers studied the relationship between the lateral deformation of the retaining structure and the ground settlement through comparative analysis of on-site monitoring data and numerical simulation and found that the maximum lateral displacement of the longer side of the diaphragm wall in the irregular foundation pit was slightly greater than that of the shorter side of the diaphragm wall (Tan *et al*. 2014, Wei *et al*. 2016). Sun *et al*. (2022) combined field observation data with numerical analysis and investigated the influence of concrete support and steel support position change on the corner effect of the internal corner. Their results showed that the lateral displacement of the diaphragm wall at the internal corner position was only related to the horizontal support structure near the corner of the pit, while the horizontal support in the middle of the pit had little influence on it. From the above studies, the current numerical simulation research considering the corner effect focuses more on the protective effect of the internal corner of the foundation pit on the diaphragm wall and surrounding structures and less on the adverse impact of the external corner of the foundation pit on the diaphragm wall.

In this paper, based on the second foundation pit project of Shenzhen Rail Transit Line 13 in Shenzhen, China, the classical Mindlin stress solution is applied to calculate the three-dimensional additional stress field of soil caused by the unloading of foundation pit excavation on both sides of existing tunnels. The existing tunnel is regarded as a Timoshenko beam on a three-parameter Kerr foundation. Considering the combined effects of the existing tunnel joints, shear stiffness, and shear soil effect, the vertical displacement control equation of the existing tunnel under additional stress load action is established. The analytical solution of vertical displacement is obtained and compared with the results of the three-dimensional numerical simulation. The special variation pattern of the displacement of existing tunnels under the influence of unloading of zero-distance foundation pits excavation on both sides of existing tunnels is summarized. Then, based on the internal corner effect and the external corner sliding surface failure mode, the foundation pit support system is optimized. The research results may provide important guidance for revealing the three-dimensional displacement characteristics of retaining structures under the influence of the pit corner effect and optimizing the design theory of similar projects.

2. Project overview

2.1 Project introduction

Shenzhen Rail Transit Line 13 North Extension Project II is one of the main components of Shenzhen's transportation network. It starts from Shangwu North Station and ends at Gongming North Station, with a total distance of 19.29 km and 11 stations. Gongming Square Station is its eighth station, located at the intersection of Changchun Middle Road and Songbai Road. It lies in a north-south direction along Changchun Middle Road, underneath the Gongming Flood Discharge Canal and the existing open-cut section of Line 6. The location of this project is shown in Fig. 1. The 7-day Hotel Building and a few residential buildings are found northeast of the station, the Gongming Post Office is northwest of the station, the Tianhong Driving School and 3-6 story buildings are

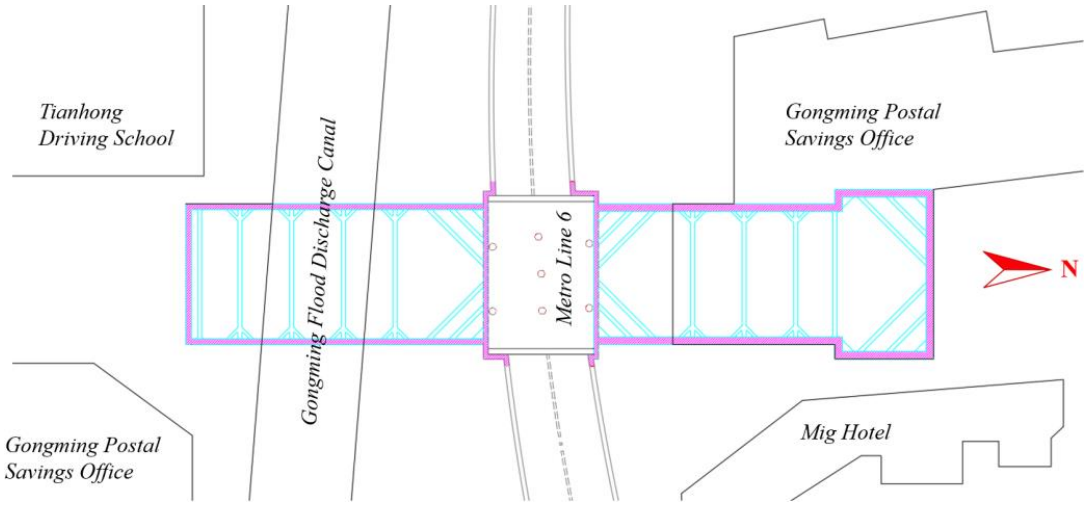

Fig. 1 Surrounding environment of the foundation pit and the first internal support

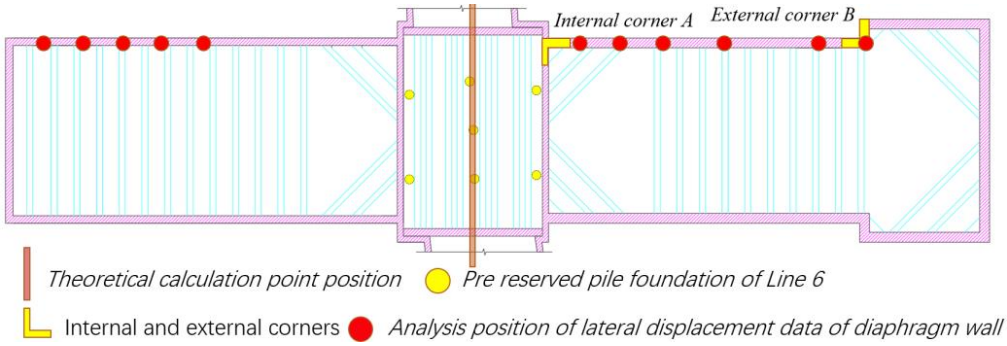

Fig. 2 Plan of the third internal support

southwest of the station, and the Tianhui City high-rise commercial and residential building is found east of the station, with a pile foundation structure. The implementation conditions of this station had been reserved in the section of Line 6. The deep and large foundation pits after excavation on both sides of the existing tunnel discussed in this study are located between the 7-day Building and Tianhong Driving School.

2.2 Geological conditions

Gongming Square Station is located in an alluvial plain area with flat terrain and ground elevation of 8.57–9.85 m. The site mainly uncovers Quaternary Holocene artificial fill, below which are Quaternary alluvial diluvium cohesive soil layers of silty clay, silty fine sand, medium coarse sand, and gravelly sand. The upper part of the bedrock is mostly covered by Quaternary residual soil, and the underlying bedrock is made of Caledonian gneiss biotite granite.

2.3 Excavation steps and support scheme

The station was constructed using a combination of open excavation method and concealed excavation method, and its layout is shown in Figs. 2 and 3. The main structural enclosure consisted of a 1 m thick diaphragm wall and internal support. The first and third concrete supports were connected to the crown beam and waist beam, respectively, at an interval of 9 m, and the second and fourth steel supports at intervals of 3 m. Six diagonal braces were used near the section of Line 6. Foundation pits I and II were open-cut sections. After the construction of foundation pit I was completed, the construction of foundation pit II was carried out. During this period, the diaphragm wall of Line 6 was taken down, and internal supports were placed simultaneously. Foundation pit II excavation and underground excavation were carried out synchronously during the mining of the cover excavation section of Line 6.

The positional relationship between the foundation pits of Line 13 and the existing tunnel Line 6 is shown in Fig. 3, which shows their cross section. The existing Gongming Square Station of Line 6 is a double-span box structure with one underground floor. During early construction, the diaphragm wall structure of Line 13, 7 temporary column piles, and the bottom section longitudinal beam had been reserved.

The system examined, shown schematically in Fig. 1 is a beam of variable cross section, carrying a so called heavy tip mass M. Its mass moment of inertia with respect to the perpendicular axis at the centroid S is denoted by JS. The publications (Abolghasemi and Jalali 2003, Younesian and Esmailzadeh 2010, Arvin and Bakhtiari-Nejad 2011) are

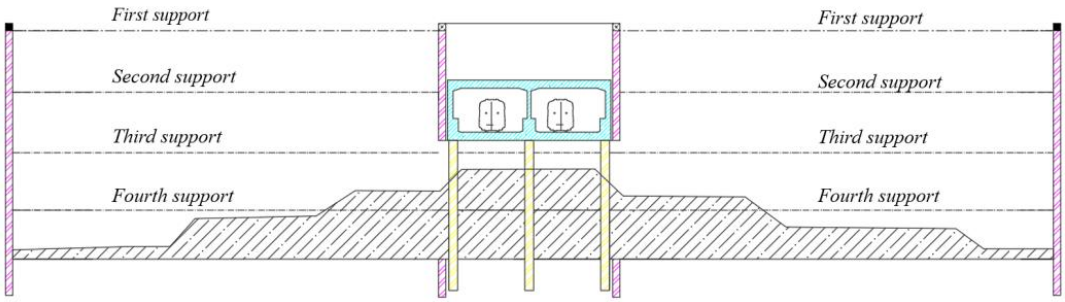

Fig. 3 Longitudinal layout of the project

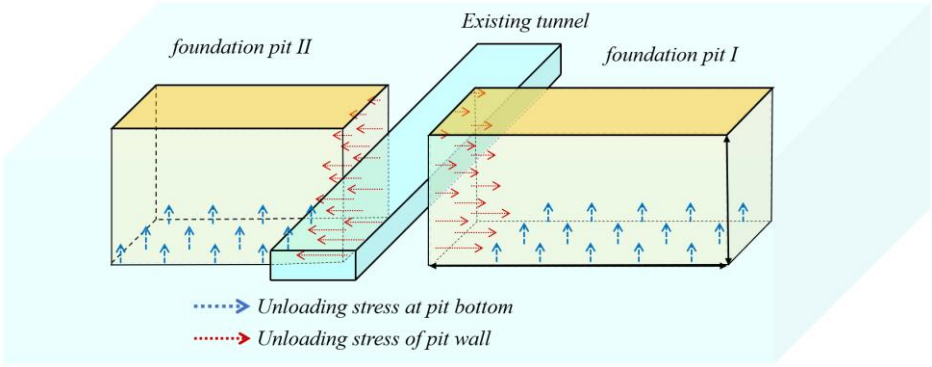

Fig. 4 Schematic diagram of the unloading effect of foundation pit excavation

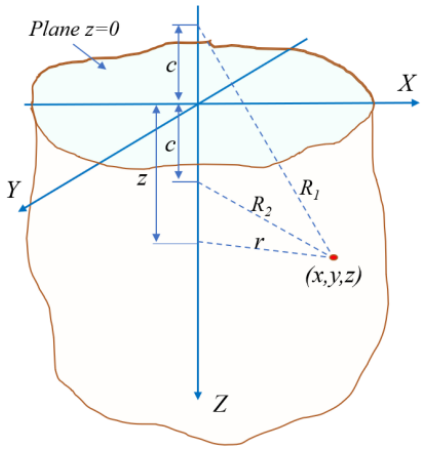

Fig. 5 Schematic diagram of Mindlin solution

considered also with rotating beams in which nonlinear oscillations are investigated. Analytical and experimental investigations on vibrating frames carrying concentrated masses with characteristics of frames have been studied by using analytical solutions and the finite element method (Cheng *et al*. 2013a, b).

3 Analytical solution of the longitudinal deformation of existing stations on a Kerr foundation

3.1 Unloading stress caused by excavation of foundation pits on both sides of the existing tunnel

In the two-stage analysis method, the first stage of foundation pit excavation can be regarded as an unloading process (Liu *et al*. 2021), which will create an additional stress field to the surrounding soil mass (Dagdeviren 2016). The vertical upward stress field generated by the unloading at the bottom of the pit will cause uplifting of the existing tunnel, while the additional load on the pit wall will make it settle. The resulting vertical displacement of the existing tunnel is due to the combined action of the two stresses (Wei *et al*. 2016), and their load relationship is shown in Fig. 4. Mindlin's vertical stress solution can be perceived as the additional vertical stress (Mindlin 1936) caused by a concentrated load acting at any position in the semi-infinite space, as shown in Fig. 5.

The Mindlin stress solution is presented in Formula (1)

$$\sigma_z^d = \frac{\gamma d}{8\pi(1-\nu)}\left[\begin{array}{l}(1-2\nu)(z_0-d)\iint_\Omega \frac{\mathrm{d}\xi\mathrm{d}\eta}{R_1^3} \\ +3(z_0-d)^3\iint_\Omega \frac{\mathrm{d}\xi\mathrm{d}\eta}{R_1^5} \\ -(1-2\nu)(z_0-d)\iint_\Omega \frac{\mathrm{d}\xi\mathrm{d}\eta}{R_2^3} \\ +\left[\begin{array}{l}3(3-4\nu)z_0(z_0+d)^2 \\ -3d(z_0+d)(5z_0-d)\end{array}\right]\iint_\Omega \frac{\mathrm{d}\xi\mathrm{d}\eta}{R_2^5} \\ +30dz_0(z_0+d)^3\iint_\Omega \frac{\mathrm{d}\xi\mathrm{d}\eta}{R_2^7}\end{array}\right], \quad (1)$$

In the above formula

$$R_1 = \sqrt{(x_1-\xi)^2+(L_0-\eta)^2+(z_0-d)^2}$$

$$R_2 = \sqrt{(x_1-\xi)^2+(L_0-\eta)^2+(z_0+d)^2}$$

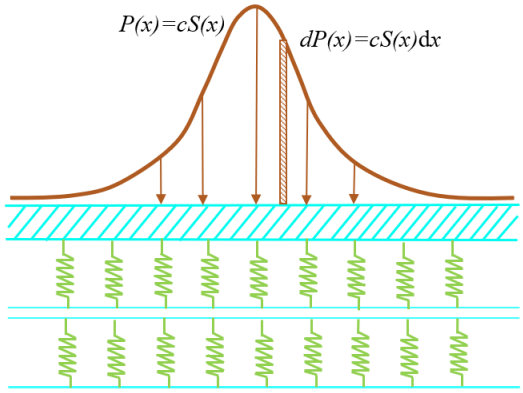

Fig. 6 Schematic diagram of the Kerr foundation model

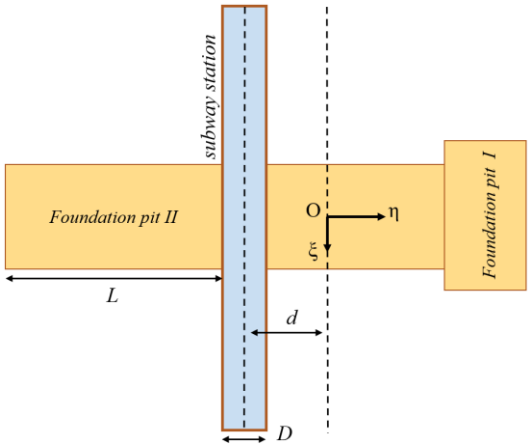

Fig. 7 Schematic diagram of the two-stage analysis method

where υ and γ are the weighted Poisson's ratio and gravity, respectively, and (x1, L0, z0) are any point on the axes of the equivalent Timoshenko beam of the tunnel. The stress field created by unloading the foundation pit on both sides can be obtained by integrating Formula (1) in the overall coordinate system. The additional stress field generated by pit wall unloading can be calculated by a similar method.

3.2 Equilibrium differential equation considering the influence of shear stiffness of the existing tunnel

The Kerr foundation model is a three-parameter model, where an elastic layer is added to the Pasternak foundation model to account for the shear effect between soil spring layers (Zhang *et al*. 2019). The parameters c and k are elastic moduli of the upper and lower elastic layers, respectively, and G is the shear modulus of the intermediate shear layer. The calculation method referred to by Zhang *et al*. (2019) was adopted, as shown in Formula (2)

$$c = 1.9k; k = \frac{4E}{3H}; G = \frac{EH}{6(1+\upsilon)}, \tag{2}$$

where E is the weighted elastic modulus of the underlying soil layer, v is the Poisson's ratio, and H is the thickness of the bottom of the beam in the foundation model, taken as 2.5 times the tunnel height. A diagram of the longitudinal section of the Kerr foundation model is represented in Fig.

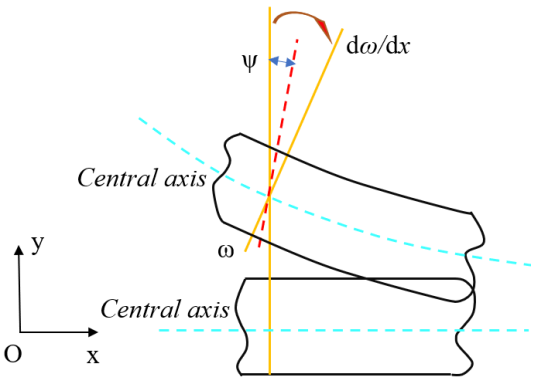

Fig. 8 Schematic diagram of the Timoshenko beam model

6. The 2-dimensional relationship between the calculated theoretical foundation pit model and the existing tunnel is shown in Fig. 7.

The following assumptions regarding the research object of this paper were made:

- Since the size of the foundation pit cannot be much larger than the section size of the existing station, and the influence of the shear stiffness of the existing station cannot be completely ignored, it is assumed that it is an infinitely long Timoshenko beam, with a width b and a height h. The deformation of the neutral axis is shown in Fig. 8. The elastic modulus is E, and the shear modulus is G. Note that the effective efficiency of longitudinal equivalent stiffness 1/7 is introduced in actual calculation because the existence of joints will weaken the stiffness of existing tunnels (Zhou *et al*. 2015);
- The tunnel bottom is attached to the foundation surface, and the tunnel deformation is equal to the deformation of the foundation model below;
- The friction between the tunnel and the foundation is ignored.

If a load p(x) is applied to the tunnel, the deflection of the tunnel under this load can be expressed as

$$w(x) = w_0 + w_1 \tag{3}$$

where w0 and w1 are the deformations of upper and lower springs, respectively. It is assumed that q0(x) and q1(x) are the spring stresses of the upper and lower layers of soil, respectively. Therefore, according to the Kerr foundation model, it can be deduced that

$$q_0(x) = cw_0 = c(w - w_1) \tag{4}$$

$$q_1(x) = kw_1 \tag{5}$$

According to the Pasternak foundation model's assumption, the relationship between shear layer deflection and stress can be expressed as

$$q_0(x) = kw_1 - G\frac{\mathrm{d}^2 w_1}{\mathrm{d}x^2} \tag{6}$$

The deflection calculation formula of the Timoshenko beam on the Kerr foundation can be obtained by combining

Formulas (3), (4), (5), and (6)

$$w = (\frac{c+k}{c})w_1 - G\frac{\mathrm{d}^2 w_1}{\mathrm{d}x^2} \tag{7}$$

The Timoshenko beam model is shown in Fig. 6 and its equilibrium differential equation is

$$-\frac{M}{EI} = \frac{\mathrm{d}^2 w}{\mathrm{d}x^2} + \frac{\left(p(x_0) - q_0(x)\right)D}{\beta AG} \tag{8}$$

When Formula (7) is substituted into Formulas (3), (4), (5), and (6) and simplified, we obtain

$$\begin{aligned} &\frac{\mathrm{d}^6 w_1}{\mathrm{d}x^6} + (\frac{Dc}{EI} + \frac{Dck}{\Phi G})\frac{\mathrm{d}^2 w_1}{\mathrm{d}x^2} - \frac{Dck}{EIG}w_1 \\ &-(\frac{c+k}{G} + \frac{Dc}{\Phi})\frac{\mathrm{d}^4 w_1}{\mathrm{d}x^4} = -\frac{Dc}{EIG}p + \frac{Dc}{\Phi G}\frac{\mathrm{d}^2 p}{\mathrm{d}x^2} \end{aligned} \tag{9}$$

Formula (8) is a sixth-order differential equation with unknown elastic layer deformation under the Kerr foundation model. The vertical deformation of the existing tunnel can be solved by substituting Formula (8) into (6).

3.3 General solution of the sixth order differential equation

If the right side of Formula (8) is equal to zero, the following formula is obtained

$$\begin{aligned} &\frac{\mathrm{d}^6 w_1}{\mathrm{d}x^6} + \left(\frac{Dc}{EI} + \frac{Dck}{\Phi G}\right)\frac{\mathrm{d}^2 w_1}{\mathrm{d}x^2} - \frac{Dck}{EIG}w_1 \\ &-\left(\frac{c+k}{G} + \frac{Dc}{\Phi}\right)\frac{\mathrm{d}^4 w_1}{\mathrm{d}x^4} = 0 \end{aligned} \tag{10}$$

Thus, Formula (9) can be converted to

$$(\frac{\mathrm{d}^2}{\mathrm{d}x^2} - \lambda_1)(\frac{\mathrm{d}^2}{\mathrm{d}x^2} - \lambda_2)(\frac{\mathrm{d}^2}{\mathrm{d}x^2} - \lambda_3)w_1 = 0 \tag{11}$$

where, $\begin{cases} \lambda_1 + \lambda_2 + \lambda_3 = (c+k)/G \\ \lambda_1\lambda_2 + \lambda_1\lambda_3 + \lambda_2\lambda_3 = Dc/EI \\ \lambda_1\lambda_2\lambda_3 = Dkc/EIG \end{cases}$

Therefore, the solution for the above equation is the same as that of the original differential equation, and the characteristic equation of Formula (10) is

$$\left.\begin{aligned} \alpha^2 - \lambda_1 \\ \alpha^2 - \lambda_2 \\ \alpha^2 - \lambda_3 \end{aligned}\right\} \tag{12}$$

The tunnel and soil stiffness data used in real practice is $\lambda 1 > 0$, therefore

$$\left.\begin{aligned} \alpha_{1,2} &= \pm\sqrt{\psi_1} = \pm\rho \\ \alpha_{3,4,5,6} &= \pm(M \pm Ni) \end{aligned}\right\} \tag{13}$$

From the above analysis, the deformation of the lower spring of the Kerr foundation model can be expressed as

$$\begin{aligned} &w_1(x) = B_1 e^{-\rho x} + B_2 e^{\rho x} + e^{-Rx}\left(B_3\cos Tx + B_4\sin Tx\right) \\ &+e^{Rx}\left(B_5\cos Tx + B_6\sin Tx\right) \end{aligned} \tag{14}$$

When $x \to \infty$, we obtain

$$w_1(x) = B_1 e^{-\rho x} + B_2 e^{\rho x} + e^{-Rx}\left(B_3\cos Tx + B_4\sin Tx\right) \tag{15}$$

3.4 Solution of equations under concentrated load

After obtaining the analytical solution for the deformation of the lower elastic layer of the Kerr foundation model under the concentrated load, the control equation for the deflection of the existing tunnel caused by foundation pit excavation can be formulated. According to the symmetry, after the local coordinate system is established at the point where the concentrated force acts, the following relationship exists at x = 0

$$\left.\begin{aligned} \frac{dw}{dx} &= 0 \\ \frac{dw_2}{dx} &= 0 \\ EI\frac{\mathrm{d}^3 w}{\mathrm{d}x^3} &= \frac{\mathrm{pD}}{2} \end{aligned}\right\} \tag{16}$$

From the above, the analytic solution under the action of concentrated force can be obtained

$$w_1(x) = C_1 e^{-\rho x} + C_2 e^{\rho x} + e^{-Rx}\left(C_3\cos Tx + C_4\sin Tx\right) \tag{17}$$

3.5 Vertical displacement solution of the existing tunnel under unloading of foundation pits on both sides

In the overall coordinate system, assuming that an additional stress dF is applied at x = x0, the analytical solution of the existing tunnel deflection under the action of the concentrated force dFdx is

$$\begin{aligned} &\mathrm{d}w(x) = C_1 e^{-\rho|x-\xi|}\mathrm{d}\xi \\ &+e^{-R|x-\xi|}(C_2\cos T|x-\xi| + C_3\sin T|x-\xi|)\mathrm{d}\xi \end{aligned} \tag{18}$$

The analytical solution of the vertical deformation of the existing tunnel can be obtained by integrating Formula (18).

$$w(x) = \int_{-\infty}^{+\infty}\mathrm{d}w(x) \tag{19}$$

4 Numerical analysis of the pit corner effect

4.1 Model description

4.1.1 Model size

The numerical simulation model was analyzed by the finite difference software Flac3D. To reduce the influence of the model boundary restrictions on the calculation

Table 1 Soil parameters in Flac3D model

	H	γ	E_{50ref}	E_{oedref}	E_{uref}	υ	f	c
	(m)	(kN/m^3)	(MPa)	(MPa)	(MPa)		(°)	(kPa)
Plain fill	3	17.5	5.0	5.0	10	0.23	8	14
Silty clay	7	18.9	3.0	3.0	10	0.33	15	20
Earthy granite	8	20.0	8.3	8.3	27.0	0.26	27	33
Moderately weathered granite	32	26.0	30.0	30.0	30	0.25	33	300

Table 2 Supporting structure parameters in Flac3D model

Supporting structure	Material	Sectional size	E/(GPa)	γ/(kN/m^3)	υ
Diaphragm wall	C35	1000	30	25	0.24
Steel support	Q235	800	210	78	0.3
Uplift pile	C35	1200	80	26	0.24
Jet grouting pile	C42.5	1200	32.5	25	0.24
Internal concrete support	C35	800×1200	30	25	0.25

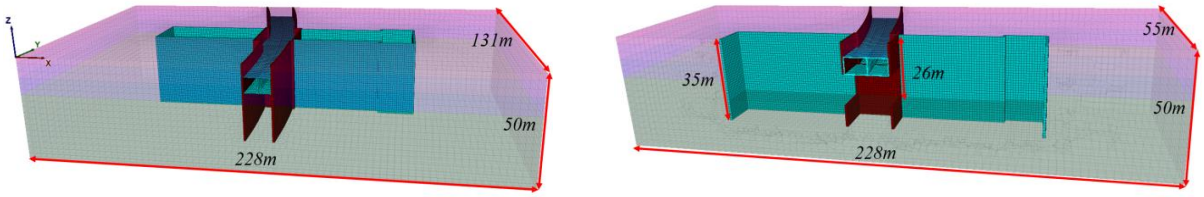

(a) Perspective view of the overall model (b) Perspective view of the half section model

Fig. 9 Numerical perspective model

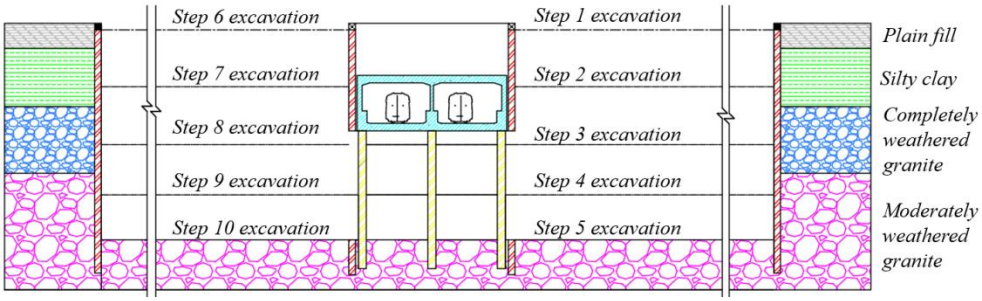

Fig. 10 Schematic diagram of construction steps

results, the excavation depth and the length of the foundation pit were doubled and used for simulation. The overall model was 228 m long, 131 m wide (with the existing tunnel length), and 50 m high. The foundation pit on the left, Foundation pit II, was 50 m long and 20 m wide. The foundation pit on the right was 57 m long, the standard section was 20 m wide, and the shield expansion section was 27 m. The maximum excavation depth was 26 m. To eliminate the size effect as much as possible, the numerical model consisted of about 440,000 elements and 340,000 nodes. The overall model dimension perspective view and the half-section perspective view are shown in Fig. 9.

4.1.2 Material parameters

The plastic-hardening constitutive model, which combines nonlinear elasticity and plasticity, is closer to the plastic theory than the Mohr-Coulomb model. Different elastic modulus values can be considered according to the loading and unloading conditions to better simulate the rebound phenomenon that happens with unloading of the pit bottom (Moradi *et al*. 2015). Therefore, the plastic hardening constitutive model was used to simulate the soil element in this paper. Tables 1 and 2 give detailed soil parameters and support structure parameters of the model.

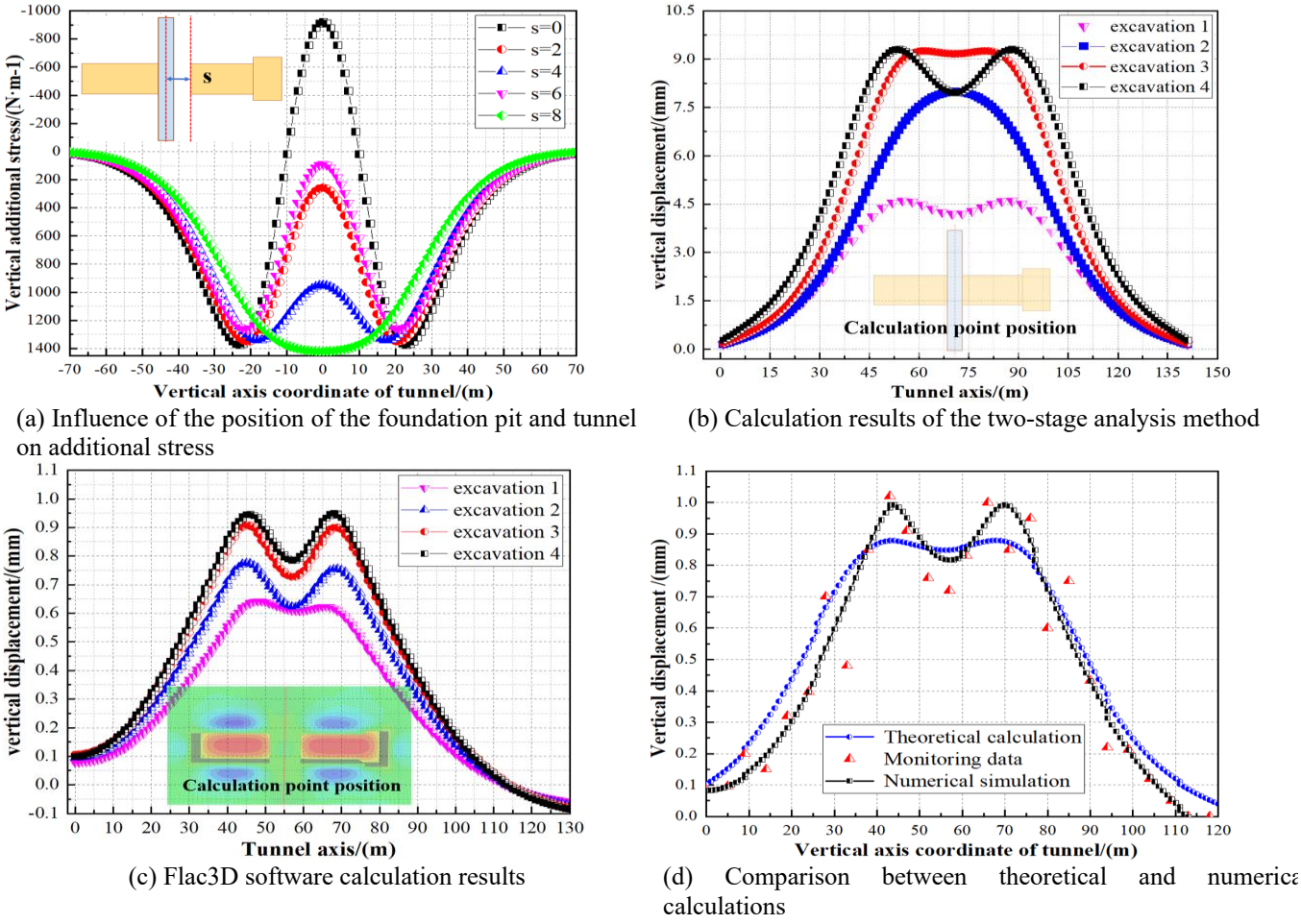

(a) Influence of the position of the foundation pit and tunnel on additional stress

(b) Calculation results of the two-stage analysis method

(c) Flac3D software calculation results

(d) Comparison between theoretical and numerica calculations

Fig. 11 Comparison diagram of vertical displacement in the construction stage

Since the demolition of the diaphragm wall was involved in the construction process, solid element and elastic constitutive models were used to simulate the diaphragm wall. Both concrete internal bracing and steel bracing were simulated by beam element and elastic constitutive models, respectively.

4.1.3 Foundation pit boundary, load conditions, and excavation process

The top surface of the model was a free surface, and the bottom surface was a fixed constraint. Normal constraints were applied to the remaining boundary surfaces. The gravitational acceleration was 9.8 m/s2. After simulating the construction process of the existing tunnel, the velocity field and displacement field were reset without considering the impact of the dynamic load of the existing operating tunnel. The demolition of the diaphragm wall was simulated without considering the effect of groundwater by null model for solid elements. The overall construction steps are shown in Fig. 10.

4.2 Comparison between numerical solution and analytical solution

Wei *et al*. (2016) pointed out that the unloading effect of the pit base would cause the tunnel to bulge and deform, and the unloading effect of the pit wall would cause settlement of the tunnel. The combined action of the two stresses would result in the vertical displacement of the existing tunnel. The load relationship is shown in Fig. 4. The final vertical displacement depends on the relative position of the foundation pit and the existing tunnel, and the closer the distance between the two, the greater the additional stress of the uplift will be. As shown in Fig. 11(a), this trend is in accordance with the results of Zhang *et al*. (2019). The numerical simulation data of the top center line of the existing tunnel were selected and compared with the Pit monitoring data and theoretical calculation results. Figs.11(b)-11(d) show the vertical displacement graph of the analytical solution and numerical solution during the excavation of foundation pit II. The overall displacement trend of the two solutions was close, and the maximum displacement was about 1 mm. The monitoring requirements stated that the absolute deformation should be less than 10 mm, indicating that the construction scheme was in line with the requirements. Fig. 11(d) shows the vertical displacement comparison of the top center line of Line 6 after the completion of the foundation pit construction. The numerical calculation agrees with the monitoring data and theoretical calculation. In the numerical simulation, the maximum displacement of the upper convex part was 0.92 mm, and the pit wall

displacement of the lower concave part was 0.79 mm. According to the theoretical calculation, the maximum displacement of the upper convex part was 0.89 mm, and the maximum displacement of the lower concave part was 0.82 mm. The main reasons for this difference were as follows:

- The influence of the support system and surrounding environment was not considered in theoretical calculation and analysis.
- The actual tunnel is a curve, but during theoretical calculation, it was straightened in the middle for simplification.
- The pit corner effect was not considered in the theoretical calculation; therefore, there may be a large margin of error when calculating the equivalent stiffness.

4.3 Numerical analysis of lateral and vertical displacement considering the influence of the pit corner effect

4.3.1 Effect of pit corner on the lateral displacement of the diaphragm wall

According to their influence on the diaphragm wall, pit corners can be divided into external corners (position B) and internal corners (position A), as shown in Figure 2. The internal corner has a protective effect on the deformation of the diaphragm wall, manifesting as the minimum lateral displacement of the diaphragm wall occurring at the internal corner (Tan *et al*. 2014). The external corner can increase the deformation of the diaphragm wall, and its failure mode is shown in Figure 14 (Szepesházi *et al*. 2016). However, existing research results have yet to fully analyze the impact of the external corner effect on the deformation of the foundation pits. Szepesházi *et al*. (2016) pointed out that the plane strain state calculation method without considering the pit corner effect could not be well applied. Only when the pit corner is symmetrically distributed, the excavation surface is long, and the load distribution is consistent, can the plane strain calculation method have high reliability. In complex cases, only engineering experience and numerical simulation can guide the design.

Ou *et al*. (2000) pointed out that the internal corner effect can be measured by plane strain ratio (PSR). When the PSR is between 0 and 0.84, the indicated area is mainly influenced by the internal corner effect. When the PSR is between 0.84 and 0.94, the indicated area is barely influenced by the internal corner effect. When the PSR is between 0.94 and 1, the indicated area is unaffected by the internal corner effect. Since the function of the external corner is opposite to the internal corner, the influence area of the external corner defined in this paper is opposite to that of the internal corner, although its spatial effect should be considered in the calculation method.

Let be the relative distance from a point at the top of the crown beam of the foundation pit to the inflection point of the edge of the foundation pit. The PSR value of this point along the z direction can then be calculated using the following formula

$$PSR = ALD / MALD \tag{20}$$

where ALD represents the average value of the lateral displacement of the diaphragm wall along the z-axis at a distance L from the pit corner, where the z-axis is in a vertically upward direction. MALD represents the average displacement near the maximum lateral displacement of the diaphragm wall.

Figs. 12(a) and 12(b) show the lateral displacement of the diaphragm wall when foundation pit II was excavated to 3 m and 26 m underground, respectively. It can be seen that when the PSR is less than 1, the displacement at the pit corner is about 1/3-1/2 of the displacement at the center, and the main influence area of the internal corner effect is about 15 m away from the pit corner. The internal corner has a protective effect on the deformation of the diaphragm wall. After the first excavation, the lateral shift of the diaphragm wall is comparable to that of a cantilever beam, and the maximum displacement occurs at the crown beam. With increasing excavation depth, the lateral deformation of the diaphragm wall becomes convex. The maximum displacement occurred near 0.17He (excavation depth of the foundation pit), and its location gradually moved downward with increasing excavation depth. The farther away from the corner, the closer PSR was to 1, and the increasing rate of PSR gradually decreased. The maximum displacement of the central area of the diaphragm wall was almost independent of the excavation depth, and always occurred at the crown beam. When excavating at the bottom of the foundation pit, the maximum lateral displacement at the pit corner was around 0.46He. Figs.12(c) and 12(d) show the lateral displacement of the diaphragm wall when foundation pit I was excavated to 3 m and 26 m underground, respectively. The deformation is restricted by the internal corner but promoted by the external corner. It can be observed that the lateral displacement at the external corner is much larger than that at the internal corner, but the main influence area is only about 15 m, which is similar to the influence area of the internal corner.

Fig. 13 shows the change in the trend of the influence coefficient of the pit corner effect with the pit corner distance at different excavation stages. When the internal corner and external corner exist at the same time, the internal corner effect is almost not affected by the excavation depth, while the PSR at the external corner gradually increases, and the maximum point of PSR gradually moves in the direction of the external corner. When there only internal corner is present, the PSR at the internal corner increases with an increase in excavation depth

4.3.2 Impact of existing stations on the pit corner effect

The cumulative lateral displacements of the diaphragm walls on both sides in each construction stage shown in Figs. 15(a) and 15(b) were selected to study the impact of the existing tunnel on the pit corner effect. The maximum displacement of the diaphragm wall near the existing tunnel was 2.4 mm, which occurred at 1/2He. The maximum displacement of the diaphragm wall on the side away from Line 6 was 5.1 mm, which occurred at the top of the foundation pit.

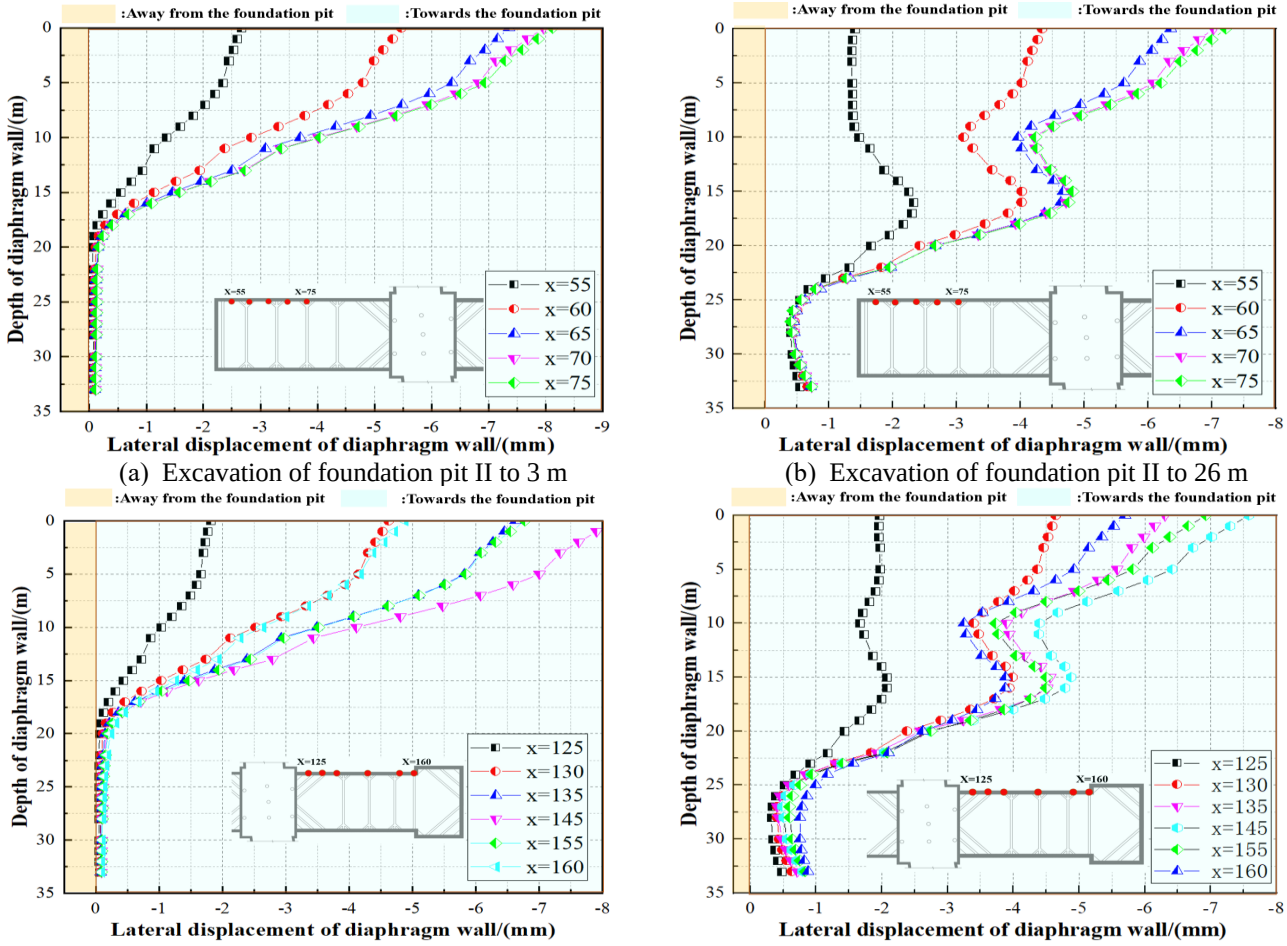

(a) Excavation of foundation pit II to 3 m (b) Excavation of foundation pit II to 26 m

(c) Excavation of foundation pit I to 3 m (d) Excavation of foundation pit I to 26 m

Fig. 12 Cumulative lateral displacement of the diaphragm wall

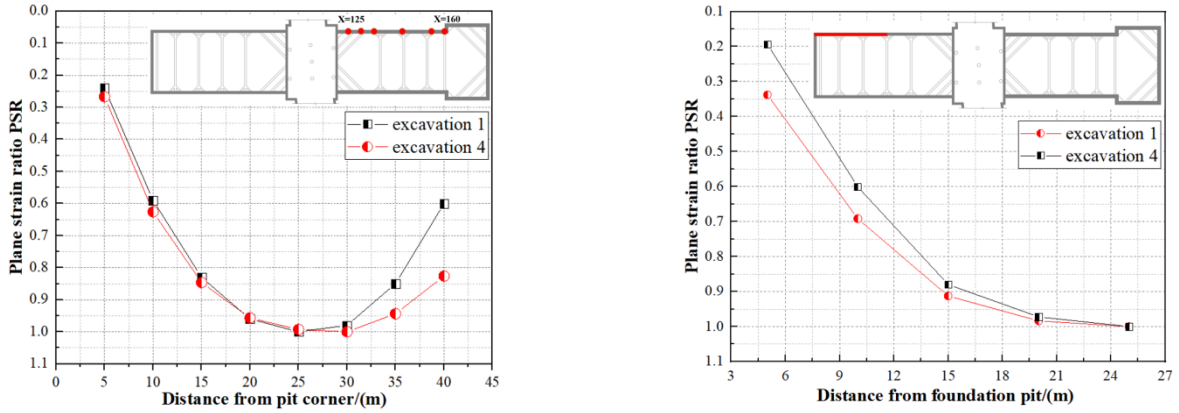

(a) Plane strain ratio in the presence of both internal and external corners (b) Plane strain ratio when only the internal corner is present

Fig. 13 Variation of influence coefficient of the pit corner effect with distance from the pit corner at different excavation stages

The influence mechanism of the existing tunnel on the pit corner effect can be summarized as follows: the presence of the existing tunnel increases the overall stiffness of the surrounding environment of the foundation pit, which leads to the reduction of the overall deformation. However, the pit corner effect could still be observed, and the affected area was about 60% of the internal corner wall.

The maximum displacement of the diaphragm wall near the tunnel side gradually rose with the increase of He, and the increasing rate gradually decreased. The maximum position of deformation of the diaphragm wall at the far tunnel side was hardly affected by He. That is, the presence of the existing tunnel lowered the point of the maximum displacement, and the stress concentration at the maximum displacement position was relieved.

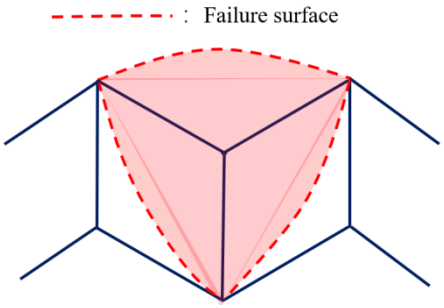

Fig. 14 Schematic diagram of the external corner sliding failure model

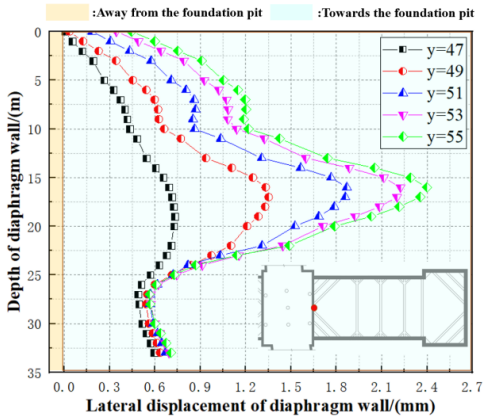

(a) Near the side of the existing tunnel

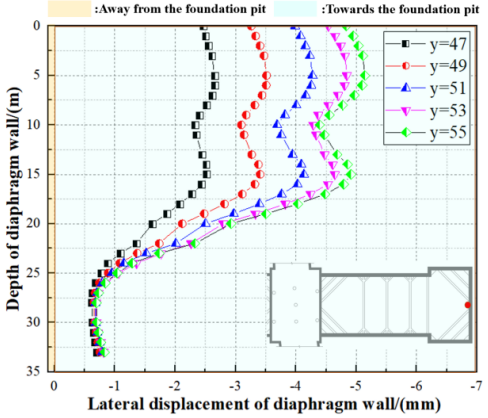

(b) The side away from the existing tunnel

Fig. 15 Cumulative lateral displacement of the diaphragm wall at each excavation stage of the foundation pit

5 Optimization design analysis based on the corner effect

5.1 Optimization of internal support design

5.1.1 Selection of the optimization scheme

According to the requirements of the monitoring scheme, the maximum absolute deformation of the diaphragm wall of Shenzhen Line 13 Project II is less than 30 mm. From Fig. 12, the maximum deformation of the diaphragm wall caused by the excavation of the foundation pits on both sides was about 8 mm, indicating that the construction scheme met the requirements. However, the pit corner effect of this scheme was evident, and too much support was used for the internal corner. Meanwhile, the support arrangement at the external corner could benefit the expected damaged surface. The internal support is optimized for economic and safety reasons. The premise of internal support optimization is to ensure that it complies with the specification requirements. Liu *et al*. (2014) pointed out that the pit corner effect on lateral displacement was mainly influenced by the thickness of soft soil layer, the ratio of excavation length to the depth, and the stiffness of the support system. Therefore, internal support optimization could begin by adjusting the following aspects: (1) internal support stiffness; (2) internal support diameter; (3) number and location of internal supports.

Since the optimization of scheme 2 fails to benefit the construction economically and will cause a substantial increase in the design workload, it was not considered. On the other hand, the internal support stiffness has a huge impact on the deformation of the diaphragm wall, and the reduction of the number of internal supports can significantly reduce construction costs. Therefore, the optimization measures in this paper adopted the combination of schemes 1 and 3.

5.1.2 Comparative analysis of support stiffness

According to the internal support scheme provided by the construction party, the first and third internal supports were 0.8 m×1.2 m concrete supports connected to the crown beam and waist beam, respectively. The second and fourth supports were steel supports with a diameter of 0.8 m each. Their parameters are shown in Table 2. Fig. 17 shows the change in cumulative maximum lateral displacement of the diaphragm wall with support stiffness under different stiffness. With increasing stiffness of the internal support, the lateral displacement first increases and then decreases. When the elastic modulus of the inner support was close to 1 GPa, the maximum displacement exceeded the monitoring requirements, seriously threatening construction safety. The elastic modulus of the concrete internal support provided by the construction party is close to the elastic modulus value of 1 GPa; therefore, the overall stiffness of the support structure should be carefully considered.

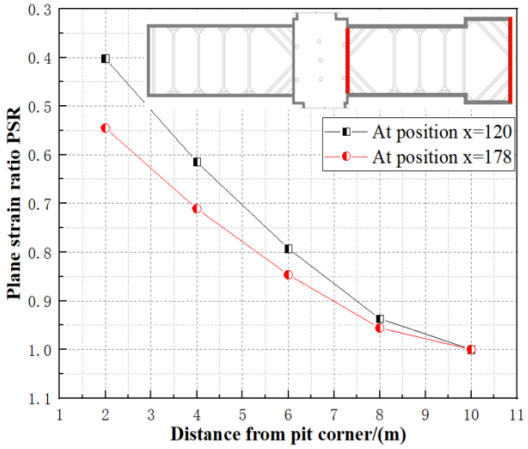

Fig. 16 Comparison between corner effect influence coefficients

5.1.3 Optimization of the support structure location

Fig. 18 shows the change in PSR under different stiffness values. With an increase in overall stiffness, the minimum value of PSR increased from 0.3 to 0.5, and the maximum displacement at the pit corner decreased gradually compared with the center of the foundation pit. However, when the elastic modulus was greater than 70 GPa, the stiffness of the inner support almost no longer reduced the influence range of the pit corner effect. Better economic and safety benefits can be achieved by adjusting the support position. It can be seen from Fig. 12 that due to the influence of the external corner, the maximum displacement position of the diaphragm wall at the north side of foundation pit 1 moved in the direction of the external corner. With the increase in excavation depth, the lateral displacement at the internal corner was only about 1/3 of that at the external corner. Therefore, the support density at the external corner should be increased, and the support density at the internal corner should be reduced. The optimized inner support position is shown in Fig. 19. The supports are uniformly spaced at 9 m, and an additional internal support is added at the external corner. Support materials and sectional area remain unchanged. Since the stiffness of the original concrete internal support is close to the danger value of stiffness, its reinforcement ratio should be increased to raise its elastic modulus to about 7 GPa.

5.1.4 Comparison of optimization results

After optimization, the lateral displacement of the diaphragm wall that is easy to produce the maximum displacement of the two foundation pits is shown in Figure 20. With the reduction in the number of internal supports, the maximum lateral displacement of the diaphragm wall is reduced to about 4 mm, which was 1/2 of that before optimization. The maximum lateral displacement position is moved from the pit top to the 4/11He position, while the support type remains unchanged. It can be seen that the maximum displacement position is mainly related to the support stiffness. Fig. 21 shows the impact coefficient and main influence areas of the pit corner effect. The foundation pit in the previous optimization stage was affected by both

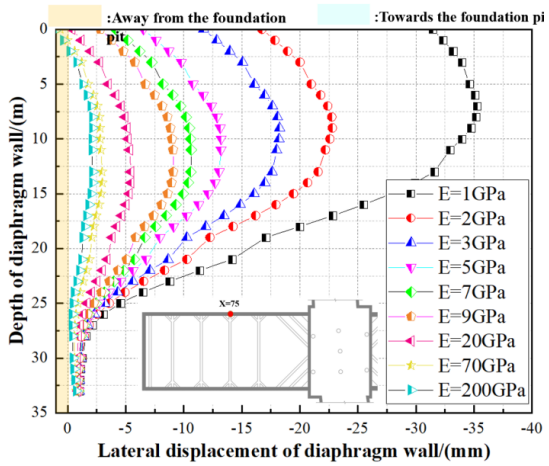

Fig. 17 Cumulative maximum displacement of the diaphragm wall under different stiffness values

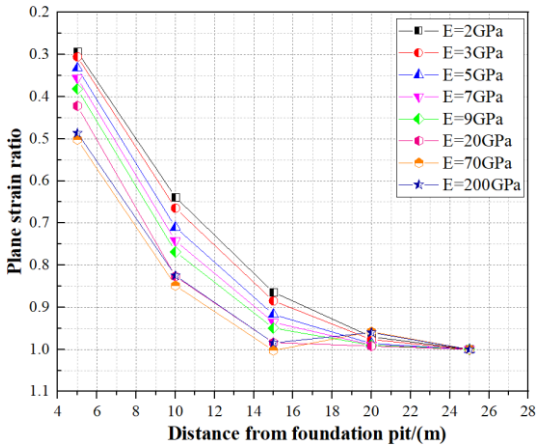

Fig. 18 Change of the influence coefficient of the pit corner effect under different stiffness values

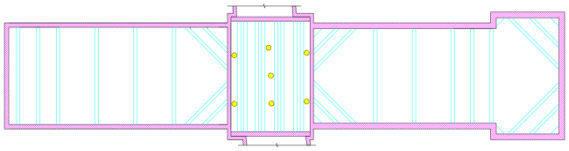

(a) First, three internal supports

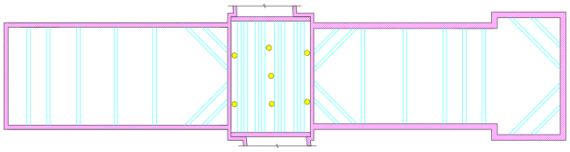

(b) Second, four internal supports

Fig. 19 Layout plan for optimized internal support

internal and external corners. The main affected area accounted for 80% of the pit wall, while only 56% was affected after optimization. The main influence area of the internal corner effect of the second stage foundation pit accounted for about 60% of the pit wall, and the main influence area after optimization accounted for 36%. Therefore, the optimization scheme can be of more benefit economically by ensuring safe construction.

6. Conclusions

Based on the foundation pit project of Gongming Square Station of Shenzhen Metro Line 13, this paper combines theoretical analysis and numerical analysis to study the impact of foundation pit excavation on the vertical displacement of existing tunnels. First, based on Mindlin's solution, the additional stress field caused by excavating deep and large foundation pits with zero distance on both sides of an existing tunnel is derived. The existing tunnel is regarded as a Timoshenko beam placed on a Kerr foundation. Considering the influence of the shear stiffness of the existing tunnel, the deformation differential equation of the tunnel under the action of the additional stress field is established, and the analytical solution of the vertical

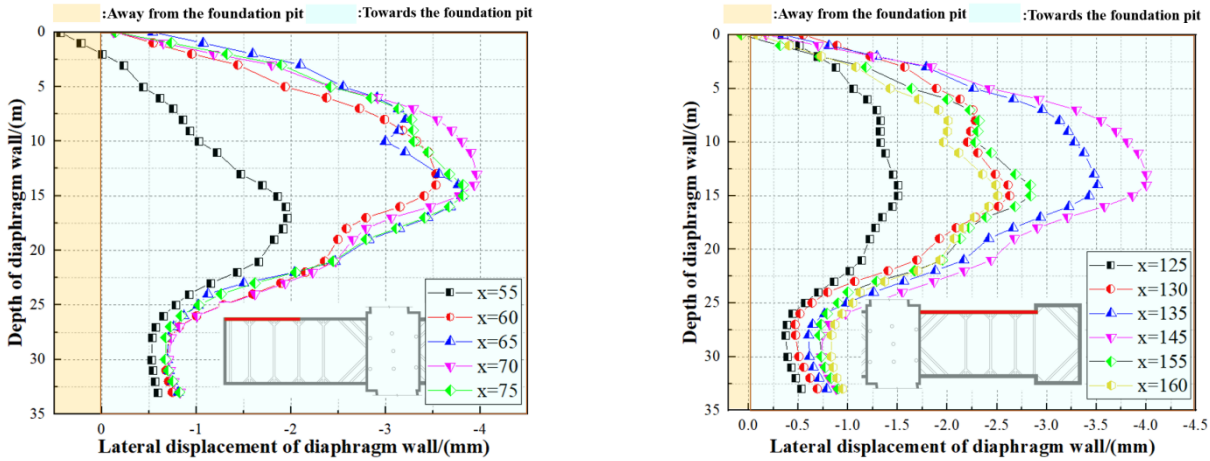

(a) Only internal corner (b) Both internal and external corners

Fig. 20 Cumulative lateral displacement of the diaphragm wall after optimization

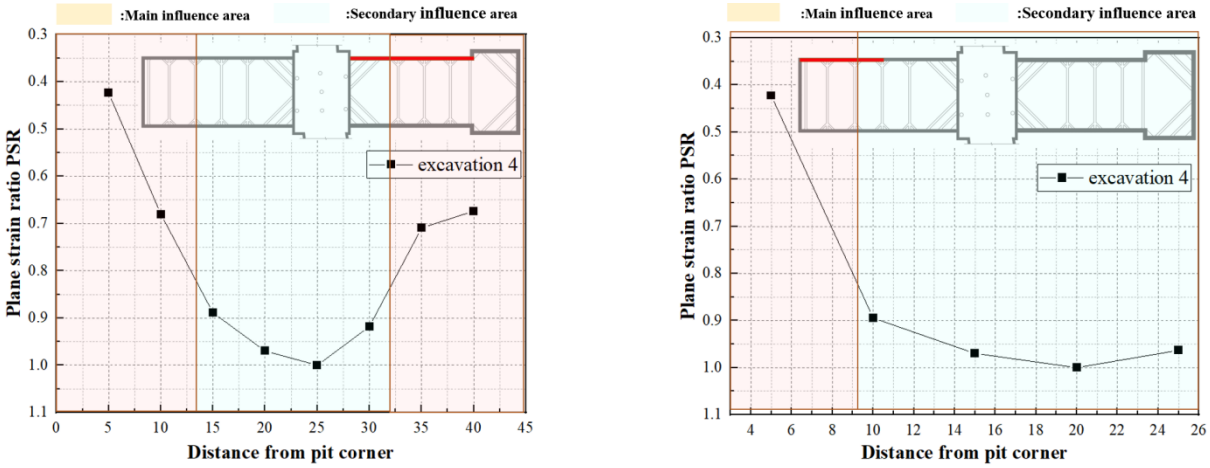

(a) Internal and external corners (b) Only internal corner

Fig. 21 Impact coefficient of the pit corner effect and main impact areas

displacement of the tunnel is derived. The impact of foundation pit excavation on the vertical displacement of the existing tunnel is analyzed by comparing the analytical results with the numerical results and monitoring data. The influence of the foundation pit's external and internal corners on the deformation of the diaphragm wall is analyzed based on the pit corner effect and external corner failure mode, and an optimal design scheme for the foundation pit support system is proposed. The main findings are as follows:

- With the decrease of the distances from the outer boundary of the foundation pit to the tunnel axis, the existing tunnel shows a trend of settlement first followed by vertical uplift deformation. When the foundation pit is closest to the existing tunnel, the uplift displacement of the tunnel reaches the maximum, and it is distributed in an "M" shape along the longitudinal direction of the tunnel. With increase in excavation depth of the foundation pit, the concave point gradually curves more.
- The overall stiffness of the foundation pit support structure greatly impacts by the pit corner effect and the deformation of the diaphragm wall. When the unified elastic modulus of the internal support is greater than 200 GPa, the maximum displacement of the diaphragm wall is less than 1 mm, and its position gradually moves downward from the ground surface with increasing excavation depth. Therefore, the existing tunnel is involved in increasing the stiffness of the surrounding environment of the foundation pit, effectively limiting the lateral shift of the diaphragm wall, but plays a minor role in reducing the extent of the main area influenced by the pit corner effect.
- During excavation of the foundation pit, the lateral displacement of the diaphragm wall at the internal corner is the smallest, which is evidently lower than the central position of the pit wall. The deformation of the pit wall presents a parabola shape towards the inner side of the foundation pit ("concave"). The internal corner has a limited deformation effect on the foundation pit diaphragm wall. The maximum lateral displacement at the external corner is three times than at the internal corner, and the external corner effect will cause stress concentration on the local diaphragm wall. The factors affecting the external and internal corner effects are the same and are mainly related to

the excavation depth, the length of the foundation pit, and the relative relationship between existing tunnels. The main area of influence of the external corner is related to the relative position of the internal corner, but the complex mechanism of the interaction between the external corner and the internal corner needs further investigation.

- Compared to the original support scheme, the proposed optimized scheme based on the pit corner effect reduces the number of supports by 17%. Based on the failure mode of the external corner sliding surface, the support position is optimized to control the main influence area of the pit corner effect. After optimization in this project, the maximum lateral displacement point of the diaphragm wall moves downward from the top of the pit wall to the 4/11He position. PSR at the internal corner increases from 0.25 to 0.45, and the main influence area of the internal corner effect decreases from 56% to 36%. This shows that the influence range of the pit corner effect can be effectively reduced by adjusting the support stiffness and support position. The main influence area of the overall pit corner effect is reduced by 64%, and the maximum overall displacement of the diaphragm wall after optimization is only 1/2 of that before optimization. The proposed optimization scheme, therefore, reduces not only construction costs but also the construction workload.

Ackonwledgments

The authors gratefully acknowledge the financial support provided by the National Natural Science Foundation of China (Nos. 51878074, 52278395, and 52078061).

References

Avcar, M., Hadji, L. and Akan, R. (2022), "The influence of Winkler-Pasternak elastic foundations on the natural frequencies of imperfect functionally graded sandwich beams", *Geomech. Eng*., **31**(1), 99-112. https://doi.org/10.12989/gae.2022.31.1.099.

Bennedjadi, M., Aldosari, S.M. and Chikh, A. (2023), "Visco-elastic foundation effect on buckling response of exponentially graded sandwich plates under various boundary conditions", *Geomech. Eng*., **32**(2), 159-177. https://doi.org/10.12989/gae.2023.32.2.159.

Cai, G., Chu, Y. and Liu, S. (2016), "Evaluation of subsurface spatial variability in site characterization based on RCPTU data", *Bull. Eng. Geol. Environ*., **75**, 401-412. https://doi.org/10.1007/s10064-015-0727-8.

Chen, S. (2020), "Study on deformation response characteristics of shield tunnel lining structure under adjacent stratum disturbance", Ph.D. Dissertation, Hunan University, Hunan.

Ding, Z., Jin, J. and Han, T.C. (2018), "Analysis of the zoning excavation monitoring data of a narrow and deep foundation pit in a soft soil area", *J. Geophys. Eng*., **15**(4), 1231-1241. https://doi.org/10.1088/1742-2140/aaadd2.

Ding, Z., Jin, J. and Han, T.C. (2018), "Analysis of the zoning excavation monitoring data of a narrow and deep foundation pit in a soft soil area", *J. Geophys. Eng*., **15**, 1231-1241. https://doi.org/ 10.1088/1742-2140/aaadd2.

Dagdeviren, U. (2016), "Shear stresses below the rectangular foundations subjected to biaxial bending", *Geomech. Eng*., **10**(2), 189-205. https://doi.org/10.12989/gae.2016.10.2.189.

Huang X., Huang H.W. and Zhang D.M. (2012), "Study on longitudinal deformation of existing shield tunnel under excavation unloading", *J. Geotech. Eng*., **34**(7), 1241-1249.

He, G., Li, X. and Lou, R. (2016), "Nonlinear FEA of higher order beam resting on a tensionless foundation with friction", *Geomech. Eng*., **11**(1), 95-116. https://doi.org/10.12989/gae.2016.11.1.095.

Huang, K., Sun, Y.W. and Yang, J.S. (2022), "Three-dimensional displacement characteristics of adjacent pile induced by shield tunneling under influence of multiple factors", *J. Central South Univ*., **29**(5), 1597-1615. https://doi.org/10.1007/S11771-022-5003-Z.

Liang, R.Z., Lin, C.G. and Tang, D. (2017), "Analysis of longitudinal deformation of adjacent tunnel due to excavation of foundation pit considering tunnel shear effect", *J. Rock Mech. Eng*., **36**(1), 223-233. https://doi.org/10.13722/j.cnki.jrme.2015.1585.

Li, Z., Cheng, K. and Zhong, C.L. (2021), "Longitudinal equivalent flexural stiffness of rectangular pipe-jacking tunnel in integrated pipe gallery", International Symposium-Asian Rock Mechanics Symposium, Beijing, China, October.

Li, D.P., Tang, D.G. and Huang, M. (2014), "Study on mechanism of space effect of deep foundation pit and soil stress considering its influence", *J. Zhejiang Univ*., **48**(9), 1632-1639.

Lin, P., Liu, P. and Ankit, G. (2021), "Deformation monitoring analysis and numerical simulation in a deep foundation pit", *Soil Mech. Found. Eng*., **58**(1), 56-62. https://doi.org/10.1007/S11204-021-09706-2.

Liu, N.W., Gong, X.N. and Yu, F. (2014), "Analysis of spatial effects in strutted excavation and related influential factors", *Rock Soil Mech*., **35**(8), 2293-2298. https://doi.org/10.16285/j.rsm.2014.08.040.

Liu, L., Wu, R. and Congress, S.S. (2021), "Design optimization of the soil nail wall-retaining pile-anchor cable supporting system in a large-scale deep foundation pit", *Acta Geotechnica*, **16**(7), 2251-2274. https://doi.org/10.1007/S11440-021-01154-4.

Lohar, H., Mitra, A. and Sahoo, S. (2019), "Nonlinear response of axially functionally graded Timoshenko beams on elastic foundation under harmonic excitation", *Curved Layered Struct*., **6**(1), 90-104. https://doi.org/10.1515/cls-2019-0008.

Liu, Z., Xue, J. and Ye, J. (2021), "A simplified two-stage method to estimate the settlement and bending moment of upper tunnel considering the interaction of undercrossing twin tunnels", *Transport. Geotech*., **29**, 1-13. 100558. https://doi.org/10.1016/J.TRGEO.2021.100558.

Limkatanyu, S., Sae-Long, W. and Hansapinyo, C. (2023). "Nonlinear shear-flexure-interaction RC frame element on Winkler-Pasternak foundation", *Geomech. Eng*., **32**(1), 69-84. https://doi.org/10.12989/gae.2023.32.1.069.

Mindlin, R.D. (1936), "Force at a point in the interior of a semi-infinite solid", *Physics*, **7**(5), 195-202. https://doi.org/10.1063/1.1745385.

Moradi, G. and Abbasnejad, A. (2015), "Experimental and numerical investigation of arching effect in sand using modified Mohr Coulomb", *Geomech. Eng*., **8**(6), 829-844. https://doi.org/10.12989/gae.2015.8.6.829.

Mei, Y., Zhou, D. and Wang, X., (2021), "Deformation law of the diaphragm wall during deep foundation pit construction on lake and sea soft soil in the Yangtze River Delta", *Adv. Civil Eng*., 2021, 1-11. https://doi.org/10.1155/2021/6682921.

Nam, K.T., Jeong, J.H. and Kim, S.H. (2022), "Measures to control deformation in deep excavation for cut and cover

tunneling", *Geomech. Eng*., **29**(3), 339-348. https://doi.org/10.12989/gae.2022.29.3.339..

Ou, C.Y., Shiau, B.Y. and Wang, I.W. (2000), "Three-dimensional deformation behavior of the Taipei National Enterprise Center (TNEC) excavation case history", *Can. Geotech. J*., **37**(2), 438-448. https://doi.org/10.1139/t00-018.

Roboski, J.F. (2004), "Three-dimensional performance and analyses of deep excavations", Ph.D.Dissertation, Northwestern University. Evanxton.

Szepesházi, A., Mahler, A. and Móczár, B. (2016), "Three dimensional finite element analysis of deep excavations' concave corners", *Periodica Polytechnica Civil Eng*., **60**(3), 371-378. https://doi.org/10.3311/PPCI.8608.

Tan, Y., Wei, B. and Diao, Y. (2014). Spatial corner effects of long and narrow multipropped deep excavations in Shanghai soft clay", *J Perform Constr Fac*., **28**(4), 1-17. https://doi.org/10.1061/(ASCE)CF.1943-5509.0000475.

Tan, J., Zheng, X. and Sun, Y. (2020), "Analysis of pit corner effect of special-shaped foundation pit of subway station", *Proceedings of the IOP Conference Series: Earth and Environmental Science*, Tokyo, Japan, October.

Wei, G. and Zhao, C.L. (2016), "Calculation method of additional load of adjacent subway tunnel caused by excavation of foundation pit", *J. Rock Mech. Eng*., **35**(1), 3408-3417. https://doi.org/10.13722/j.cnki.jrme.

Wang, Z., Shi, C. and Gong, C. (2022), "Difference solutions for responses of foundation-beams with arbitrary boundary conditions considering spatial soil variability and its applications", *Comput. Geotech*., **151**, 1-12. https://doi.org/10.1016/j.compgeo.2022.105002.

Xia, G.Y. (2022), "Generalized foundation Timoshenko beam and its calculating methods", **92**(3), 1015-1036. https://doi.org/10.1007/S00419-021-02090-1.

Zhou, Z.L., Chen, S.G. and Chen, L. (2015), "Simplified theoretical analysis of the influence of foundation pit construction on the uplift deformation of underground subway tunnel", *J. Geotech. Eng*., **37**(12), 2224-2234.

Zhang, D.M., Huang, Z.K. and Li, Z.L. (2019), "Analytical solution for the response of an existing tunnel to a new tunnel excavation underneath", *Comput. Geotech*., **108**, 197-211. https://doi.org/10.1016/j.compgeo.2018.12.026.

Zhang, Z., Zhang, C. and Jiang, K. (2019), "Analytical prediction for tunnel-soil-pile interaction mechanics based on Kerr foundation model", *J. Civil Eng*., **23**(6), 2756-2771. https://doi.org/10.1007/s12205-019-0791-x.

Zhang, Z.G., Jiang, K.M. and Wang, Z.W. (2020), "Theoretical analysis of longitudinal deformation of existing tunnel induced by foundation pit excavation considering Pasternak foundation model", *Tunnel Constr*., **40**(1), 57-67.

Zhang, Y.W., Ding, H.X. and She, G.L. (2023), "Wave propagation of CNTRC beams resting on elastic foundation based on various higher-order beam theories", *Geomech. Eng*., **33**(4), 381-391. https://doi.org/10.12989/gae.2023.33.4.381.